ELSEVIER

Magnetic Resonance Imaging 22 (2004) 139–148
Original Contributions

MAGNETIC RESONANCE IMAGING

MRI diffusion tensor reconstruction with PROPELLER data acquisition

Arvidas B. Cheryauka[a,*], James N. Lee[a], Alexei A. Samsonov[b], Michel Defrise[c], Grant T. Gullberg[d]

[a]*Center for Advanced Medical Technologies, Radiology Department, University of Utah, Salt Lake City, UT 84108, USA*
[b]*Scientific Computing and Imaging Institute, School of Computing, University of Utah, Salt Lake City, UT 84108, USA*
[c]*Division of Nuclear Medicine, AZ-VUB University Hospital, Vrije Universiteit Brussel, Brussels, Belgium*
[d]*Department of Nuclear Medicine and Functional Imaging, E. O. Lawrence Berkeley National Laboratory, Berkeley, CA 94720, USA*

Received 1 March 2003; received in revised form 2 August 2003; accepted 3 August 2003

Abstract

MRI diffusion imaging is effective in measuring the diffusion tensor in brain, cardiac, liver, and spinal tissue. Diffusion tensor tomography MRI (DTT MRI) method is based on reconstructing the diffusion tensor field from measurements of projections of the tensor field. Projections are obtained by appropriate application of rotated diffusion gradients. In the present paper, the potential of a novel data acquisition scheme, PROPELLER (Periodically Rotated Overlapping ParallEL Lines with Enhanced Reconstruction), is examined in combination with DTT MRI for its capability and sufficiency for diffusion imaging. An iterative reconstruction algorithm is used to reconstruct the diffusion tensor field from rotated diffusion weighted blades by appropriate rotated diffusion gradients. DTT MRI with PROPELLER data acquisition shows significant potential to reduce the number of weighted measurements, avoid ambiguity in reconstructing diffusion tensor parameters, increase signal-to-noise ratio, and decrease the influence of signal distortion.

1. Introduction

MRI diffusion imaging has demonstrated many important applications in diagnostic medicine. This method has proved to be effective in measuring the diffusion tensor field in brain [1], cardiac [2], and spine [3] imaging. In particular, diffusion tensor (DT) MRI offers significant potential for studying the fiber structure of tissues. Recently, a new method, diffusion tensor tomography MRI (DTT MRI), was proposed in which the tensor field is reconstructed from measurements of projections of the tensor field [4–6]. The tensor tomography approach assumes that a proper collection of projected scalar measurements can be obtained to form an adequate dataset for reconstruction of the full tensor field or, at least, of its principal directions [7]. This method used in combination with PROPELLER (Periodically Rotated Overlapping ParallEL Lines with Enhanced Reconstruction) acquisition has the potential to reduce the number of measurements or improve the signal-to-noise ratio (SNR) for the same number of measurements used presently in DT MRI.

For many years, sampling of the MR signals on a uniform and rectangular Cartesian grid in *k*-space has been the most popular acquisition method. It is motivated by use of an easy image reconstruction technique that applies the Fast Fourier Transform (FFT), which has become the standard tool in integrated software toolkits such as Matlab (MathWorks, Natick, MA) and IDL (Research Systems, Inc., Denver, CO).

At present, nonuniform sampling schemes including radial [8], spiral [9], rosette [10], PROPELLER [11], or random [12] acquisitions are gaining importance in various MRI applications. The image reconstruction techniques for arbitrary nonregular grids can be divided into two groups. The first group, regridding methods, provides computationally inexpensive resampling and interpolation of a kernel function into a uniform Cartesian grid. The second group includes optimization methods that minimize a least-squares cost functional. The optimization methods can handle nonuniform coil sensitivity and off-resonance effects, improve noise suppression, and provide a robust solution within a larger parametric domain [13–15]. In clinical applications, imaging methods with nonuniform

* Corresponding author. Tel.: +801-536-4653.
E-mail address: Arvi.Cheryauka@med.ge.com (A. Cheryauka).

0730-725X/04/$ – see front matter
doi:10.1016/j.mri.2003.08.001

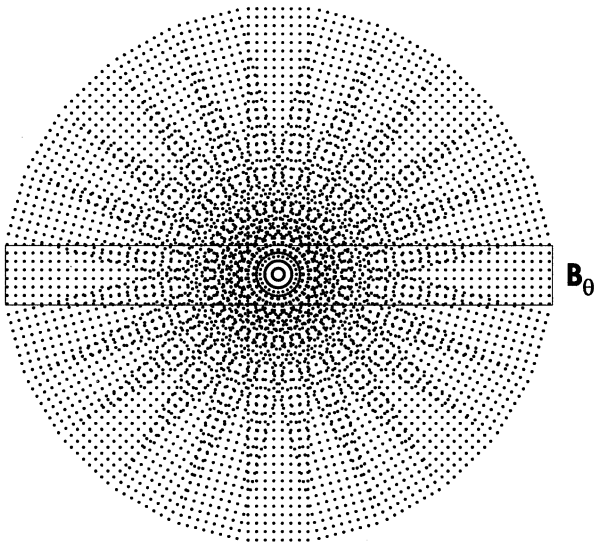

Fig. 1. An example of PROPELLER *k*-space. It contains 12 uniform sampled blades with 256 and 32 encodings in readout and phase directions, respectively.

acquisition schemes have proved their capability to suppress noise and to reduce the artifacts caused by motion and by eddy currents in functional [16], cardiac [11], arterial [17], and spine [18] imaging as well as others.

The purpose of the present paper is to examine the potential of combining the PROPELLER data acquisition scheme with DTT. First, the conventional regridding and FFT algorithm for the PROPELLER acquisition is presented. Then the Papoulis-Gerchberg iterative extrapolation algorithm is implemented for incomplete sampling to reduce the number of acquisition samples. After extrapolating each diffusion-weighted image, the image formation follows by the conventional FFT algorithm. Then taking a different point of view, the DTT reconstruction can be considered as a solution to an inverse problem that evaluates DT parameters directly. The approach implemented with PROPELLER acquisition can be applied for arbitrary *k*-space sampling and is not limited by diffusion gradient directions for any PROPELLER blade. For this case, we present an iterative optimization algorithm for data acquired with PROPELLER acquisition with rotated diffusion gradients. The proposed algorithms are applied to both simulated and MRI-acquired data. The DTT method utilizing PROPELLER with rotating gradients is compared to the conventional DTI using computer-generated cardiac phantom data.

2. PROPELLER acquisition

Data collection for DTT MR imaging is based on the PROPELLER method proposed in Ref. 11. The resulting *k*-space trajectories are shown in Fig. 1. *K*-space is filled out by rotating blades around the *k*-space center. The sample spacing in the readout direction satisfies the Nyquist criterion. The number of phase encodings in each blade and the total number of blades are such that the pattern covers the whole of *k*-space without gaps.

The governing idea of PROPELLER is that the circular region at the center is overlapped by many blades. Due to this redundancy, effective data correction can be performed to reduce motion artifacts and to improve the SNR because blades overlap in the vicinity of the *k*-space center, and this can be used to average the signal.

To estimate the diffusion tensor in each voxel, one has to collect a sufficient amount of diffusion-weighted data. The PROPELLER method offers an opportunity to choose the diffusion gradient direction while acquiring each *k*-blade. The conventional approach is to acquire a full set of PROPELLER data with a fixed direction of the diffusion gradient and to reconstruct the corresponding component of the tensor. By repeating this for three (in two dimensions) or six (in three dimensions) appropriately chosen directions, the whole tensor can be recovered. An alternative approach consists in rotating the diffusion gradient simultaneously with the rotating *k*-blade. This method is flexible and might provide more complete information to reconstruct the DT. It offers a potential to reduce the total amount of diffusion-weighted data without degrading the accuracy of the reconstructed image.

3. Reconstruction methods

According to several simplifying assumptions [19], the diffusion-weighted image reconstructed from a complete set of *k*-space samples $P_\omega(\mathbf{k})$ measured with a fixed direction $\vec{\omega}$ of the diffusion gradient can be modeled as

$$\begin{aligned} p_\omega(\mathbf{r}) &= (\mathcal{F}^{-1}P_\omega)(\mathbf{r}) \\ &= \int_\Omega P_\omega(\mathbf{k})e^{-2\pi j\mathbf{k}\cdot\mathbf{r}}d\mathbf{k} \\ &= \rho(\mathbf{r})e^{-b[\vec{\omega}^T\cdot\mathbf{D}(\mathbf{r})\cdot\vec{\omega}]}, \end{aligned} \tag{1}$$

where ρ is the proton density, $\mathbf{D}$ is a second-order diffusion tensor, and

$$b = (\gamma G\delta)^2\left[\Delta - \frac{\delta}{3}\right], \tag{2}$$

is a function of the amplitude G, width δ, and spacing Δ of the diffusion gradients [20]. The constant γ is the spin gyromagnetic ratio. In Eq. 1, Ω is the support of the Fourier transform of p_ω.

For a PROPELLER acquisition, we define the region of *k*-space covered by one blade by B_θ, where the subscript θ refers to the direction of the read-out gradient for this blade. The spatial image $\tilde{p}_\omega(\mathbf{r},\theta)$ obtained from this blade is then:

$$\tilde{p}_\omega(\mathbf{r},\,\theta) = \int_{B_\theta} P_\omega(\mathbf{k})e^{-2\pi j\mathbf{k}\cdot\mathbf{r}}d\mathbf{k}, \tag{3}$$

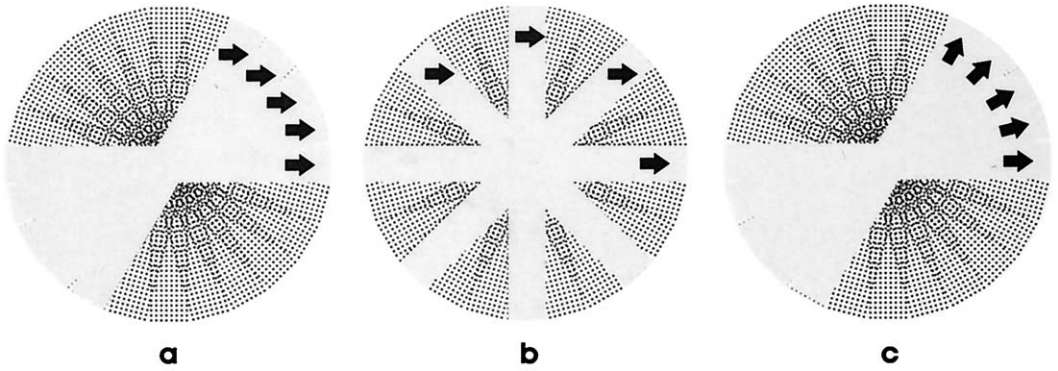

Fig. 2. Diffusion gradient encoding schemes. (a) Diffusion gradient direction is the same for all blades (for regridding + FFT algorithm). (b) Gradient direction is the same for a specific set of blades (for iterative extrapolation algorithm). (c) Gradient direction is different for each blade, rotated with the blade (for iterative optimization algorithm).

where $\vec{\omega}$ is the direction of the diffusion gradient. The images $\tilde{p}_{\omega}(\mathbf{r},\theta)$ have low resolution in the direction orthogonal to $\vec{\theta}$ but they can be used for fast testing and for identifying a region of interest (ROI) before a final high-resolution reconstruction.

The blade data should be corrected for phase inconsistency before being combined to form the complete image. The application of diffusion gradients and the motion of the object and equipment can cause significant displacement of the actual center of the *k*-blade spectrum from its formal value. We apply a phase correction algorithm for each blade by locating its signal maximum, then adjusting the intensity of the blade and its position in *k*-space. This correction procedure prevents blurring and shadowing in the reconstructed images.

The DT is a symmetric tensor depending on the voxel location **r,** and it can be expressed in terms of Cartesian coordinates as

$$D^{(2)}(\mathbf{r}) = \begin{pmatrix} D_{xx}(\mathbf{r}) & D_{xy}(\mathbf{r}) \\ D_{yx}(\mathbf{r}) & D_{yy}(\mathbf{r}) \end{pmatrix},$$

$$D^{(3)}(\mathbf{r}) = \begin{pmatrix} D_{xx}(\mathbf{r}) & D_{xy}(\mathbf{r}) & D_{xz}(\mathbf{r}) \\ D_{yx}(\mathbf{r}) & D_{yy}(\mathbf{r}) & D_{yz}(\mathbf{r}) \\ D_{zx}(\mathbf{r}) & D_{zy}(\mathbf{r}) & D_{zz}(\mathbf{r}) \end{pmatrix} \quad (4)$$

and has three (in two dimensions) and six (in three dimensions) independent components, which can be diagonalized to obtain the principal diffusivities and the corresponding principal directions at each voxel. This diagonalization can be done analytically or using a least-square method, which is more robust for noisy real-world data acquisitions.

The choice of a fixed or moving diffusion encoding unit vector $\vec{\omega}$ determines the method of reconstruction of the DT at image voxels.

3.1. Conventional gridding algorithm

We first consider the case where a complete PROPELLER data set is measured with a fixed direction $\vec{\omega}$ of the diffusion gradient (Fig. 2a). These data consist of a set of irregularly spaced *k*-space samples $P_{\omega}(k_{x,i},k_{y,i}), i = 1, \ldots, M$, and can be reconstructed using a standard gridding procedure to estimate the diffusion weighted image $p_{\omega}(\mathbf{r})$ in Eq. 1. The reconstruction consists of two steps:

1. Interpolate the irregular *k*-space samples $P_{\omega}(k_{x,i},k_{y,i})$ onto a $N \times N$ Cartesian grid, $(k_x, k_y) = (i, j)$, $i, j = 1, \ldots, N$.
2. Apply the inverse two-dimensional FFT to $P_{\omega}(i, j)$, $i, j = 1, \ldots, N$.

We summarize for completeness the gridding procedure [21], neglecting in the rest of this section the fixed subscript $\vec{\omega}$. Represent the set of sampled PROPELLER data by a function

$$P_S(k_x, k_y) = P(k_x, k_y) \cdot S(k_x, k_y), \quad (5)$$

where the sampling function S is

$$S(k_x, k_y) = \sum_{i=1}^{M} \delta^{(2)}(k_x - k_{x,i}, k_y - k_{y,i}), \quad (6)$$

is a set of Dirac impulses at the N *k*-space samples $k_{x,i},k_{y,i}$, $i = 1, \ldots, M$ located on the irregular grid defined by the PROPELLER blades. In the gridding procedure, an interpolated spectrum is defined by convolving the sampled data with some spectral window function C. To compensate for an undersampling/oversampling weighting in $S(k_x,k_y)$, we define an area density function $W(k_x,k_y)$ as

$$W(k_x, k_y) = S(k_x, k_y) * C(k_x, k_y). \quad (7)$$

The corrected *k*-space dataset results in

$$P_C(k_x, k_y) = \left\{ \left[\frac{P_S(k_x, k_y)}{W(k_x, k_y)} \right] * C(k_x, k_y) \right\} \cdot \sum_{i,j=1}^{N} \delta^{(2)}(k_x - i, k_y - j). \quad (8)$$

The corresponding reconstructed image p_C is given by the inverse Fourier transform of P_C

$$p_C(x,y) = \{[(p(x,y)*s(x,y))*^{-1}(s(x,y)\cdot c(x,y))]$$

$$\cdot\, c(x,y)\}* \sum_{i,j=1}^{N} \delta^{(2)}(x-i, y-j), \tag{9}$$

where $*^{-1}$ operation refers to a deconvolution. Finally, the transformed data are divided by $c(x,y)$ to compensate for roll-off in the inverse Fourier transform of $C(k_x,k_y)$.

$$p_C(x,y) = p_C(x,y)/c(x,y). \tag{10}$$

In our work, we have developed an efficient regridding procedure taking into account the numerical implementation experience in Refs. 21 and 22. The important part of the algorithm is a choice of convolution window function. The Kaiser-Bessel window was used. In one dimension, the discrete Kaiser window function has the form

$$C(k)=\begin{cases} I_0\left(B\sqrt{1-\left(\frac{k}{L}\right)^2}\right)/I_0(B), & \text{if } -L\le k\le L,\\ 0, & \text{otherwise,}\end{cases} \tag{11}$$

where L is window length, and I_0 is the 0^{th}-order modified Bessel function of the 1^{st} kind. The determination of an optimal value of B is similar to that described in Ref. 22.

A rotating vector $\vec{\omega}$ can potentially provide more complete information about model parameters, make reconstruction more stable, and/or require a smaller dataset for the same image quality. Such results were observed earlier in ultrasonic transmission tomography for studying anisotropic composite materials [23]. It has also been proposed for DT MR imaging [25]. In the present paper this idea is extended to a two-dimensional PROPELLER acquisition technique.

3.2. Papoulis-Gerchberg iterative extrapolation algorithm

The amount of data acquired in a PROPELLER acquisition can be reduced by collecting for each direction $\vec{\omega}$ of the diffusion gradient only a subset of the blades, as shown in Fig. 2b. In two dimensions, for instance, we need three directions $\vec{\omega}$ to recover the DT, such as $\vec{\omega}^1 = (1,0)$, $\vec{\omega}^2 = (0,1)$, and $\vec{\omega}^3 = (1/\sqrt{2}\ ,1/\sqrt{2}\ )$. One way to reduce the data size would then consist in acquiring only one out of three blades with each direction ω^{i}. We denote by $B^{\text{i}} \subset \Omega$, $i = 1, 2, 3$ the region of k-space covered by the blades acquired with a diffusion gradient along ω^{i}.

Due to the redundancy of the blades at k-space center, the low frequency components of $p_{\omega^i}(\mathbf{r})$ can still be accurately recovered from these incomplete data in B^{i}. At higher frequencies, however, data are missing in triangular shaped gaps in k-space, as shown in Fig. 2b. An accurate reconstruction of $p_{\omega^i}(\mathbf{r})$ therefore requires extrapolating the measured signal $P_{\omega^i}(\mathbf{k}),\mathbf{k} \in \mathrm{B}^{\text{i}}$ into the gaps $\Omega - B_{\text{i}}$. This problem is an example of the general ill-posed problem of extrapolating band-limited signals. These problems are ill-posed but a solution can be obtained by relying on the prior knowledge that the inverse Fourier transform of the signal has a bounded support. Thus, in our case, we know that $p_{\omega^i}(\mathbf{r}) = 0$ outside some region $\mathbf{r} \in \mathrm{Q}$ determined by the imaging FOV.

Denoting by $\tilde{P}^i_n(\mathbf{k}),\mathbf{k} \in \Omega$ the estimated extrapolated data at iteration n, the Gerchberg and Papoulis algorithm [24] proceeds by alternatively modifying the data in k-space and in image space. Starting with

$$\tilde{P}^i_0(\mathbf{k}) = 0,\ \mathbf{k} \notin B^i, \tag{12}$$

each iteration consists of three steps,

1. In k-space, substitute the measured data in the sampled region B^{i}:

$$\begin{aligned}\tilde{P}^i_{n+1}(\mathbf{k}) &= P^i(\mathbf{k}) \quad \mathbf{k}\in B^i\\ &= \tilde{P}^i_n(\mathbf{k}) \quad \mathbf{k}\notin B^i\end{aligned} \tag{13}$$

2. Take the inverse Fourier transform and truncate the resulting image outside the known support Q:

$$\begin{aligned}\tilde{p}^i_{n+1}(\mathbf{r}) &= (\mathcal{F}^{-1}\tilde{P}^i_{n+1})(\mathbf{r}) \quad \mathbf{r}\in Q\\ &= 0 \quad \mathbf{r}\notin Q\end{aligned} \tag{14}$$

3. Take the Fourier transform to get the next estimate of the signal,

$$\tilde{P}^i_{n+1}(\mathbf{k}) = (\mathcal{F}\tilde{p}^i_{n+1})(\mathbf{k}) \tag{15}$$

The stopping criterion is determined by a small positive threshold ε

$$\|\tilde{\mathbf{P}}^i_{n+1} - \tilde{\mathbf{P}}^i_n\|_{L_2} < \varepsilon. \tag{16}$$

After stopping the iteration at the N-th step, the component of the DT is recovered from Eq. 1 as

$$\vec{\omega}_i^T\mathbf{D}(\mathbf{r})\vec{\omega}_i = -\frac{1}{b}\log\frac{1}{\rho(\mathbf{r})}\,\mathcal{F}^{-1}\,(\tilde{P}^i_N)(\mathbf{r}). \tag{17}$$

3.3. Iterative optimization algorithm

An iterative optimization algorithm was developed to reconstruct the diffusion tensor $\mathbf{D}$ from a PROPELLER acquisition with rotating gradients (Fig. 2c). Under circumstances of noisy acquisition and data incompleteness, this problem has a nonunique and ill-conditioned solution. Regularization methods should be applied to impose the desirable properties to the solution. Schematically, a least-squares inversion technique for minimizing the cost functional L can be expressed as

$$L = \|\mathbf{W}_P(\mathbf{P} - \tilde{\mathbf{P}})\|_{L_2} + \alpha L^{prior}(\mathbf{W}_D\mathbf{D}), \tag{18}$$

where $\mathbf{P},\tilde{\mathbf{P}}$ are measured and predicted MR data, $\mathbf{W}_P,\mathbf{W}_D$ are data and model parameter weighting matrices, respectively, L^{prior} is a stabilizing functional carrying the specific constraint information, and α is a regularization parameter. Because the signal contains in-phase and out-of-phase components, the norm in Eq. 18 denotes a complex conjugate

expression. For simplicity, in this implementation we use identity weighting matrices $\mathbf{W}_P$ and $\mathbf{W}_D$. In iterative numerical realization the minimization problem results in a converging sequence $\{L\}_n$

$$\min\{\|\mathbf{P} - \mathcal{F}\{\rho(\mathbf{r})\exp[-b\mathbf{P}(\mathbf{m}_n)]\}\|^2 + \alpha_n L^{prior}(\mathbf{m}_n)\},$$
$$n = 1, \cdots, N, \tag{19}$$

where $\mathbf{m} = [D_{xx}, D_{yy}, D_{xy}]$ is the vector of unknowns composed of DT values within an ROI. The symbols n and N are the iteration index and total number of iterations, respectively. At each iterative step we solve a linearized problem using the regularized conjugate gradient method. The determination of the regularization parameter α_n at each iteration uses an explicit noise estimation technique [25]. An important aspect of solving linearized inverse problems is to compute a Jacobian matrix, which is composed of first derivatives with respect to components of the vector of unknowns (DT components). The derivative over the signal acquired within each blade with specific direction of diffusion-weighted gradient $\vec{\omega}$ can be expressed as follows

$$\frac{\partial P_\omega}{\partial D_{ij}(\mathbf{r})} = \mathcal{F}[p_\omega(\mathbf{r})(-b\omega_i\omega_j\delta_{i,j})],$$
$$\delta_{i,j} = \begin{cases} 1, & \text{if} \quad i = j, \\ 2, & \text{if} \quad i \neq j. \end{cases} \tag{20}$$

where p_ω is the diffusion-weighted image in Eq. 1.

If the length of the vector **m,** N_m, is less than the number of data samples N_d in the vector **P,** the conjugate gradient converges to the least-squares solution ($N_m < N_d$, overdetermined problem). For underdetermined problems, where $N_m > N_d$, the conjugate gradient iterations converge to the minimum norm solution.

The stabilizing functional L was implemented as a global total variation (TV) functional [26]

$$L(m) = \int_{ROI} |\nabla m| dx dy, \tag{21}$$

where function m is a continuous analog of the vector **m.** The advantage of the TV stabilizer is that the function $m(x,y)$ need not be differentiable, i.e., discontinuities in the spatial distribution of the material properties (DT tensor components) are allowed.

4. Results

4.1. Spin density imaging

We have tested the algorithm described above for the case of a constant (zero) diffusion gradient. We have applied the direct (regridding + FFT-based) technique using numerical and realistic phantom data to reconstruct the two-dimensional proton density function $\rho(\mathbf{r})$, defined in Eq. 1.

First, we verified the reconstruction algorithm using purely synthetic data. The original target is the well-known Shepp-Logan phantom, which contains 10 ellipses of various intensity and geometry. Its Fourier domain spectrum can be calculated analytically with any desired accuracy. The resulting Fourier spectrum of the Shepp-Logan phantom is the sum of the ellipse's spectra. The Fourier spectrum of an inclined ellipse can be found, for instance, in Ref. 14:

$$\mathrm{P}(\mathrm{k}, \theta) = \sum_{i=1}^{10} \mathrm{P}_i(\mathrm{k}, \theta),$$
$$\mathrm{P}_i(\mathrm{k}, \theta) = \rho_i \mathrm{A}_i \mathrm{B}_i \exp[-j2\pi k t_i \cos(\gamma_i - \theta)] \frac{J_1(2\pi a_i(\theta)\, k)}{a_i(\theta)\, k},$$
$$t_i = \sqrt{x_i^2 + y_i^2}, \quad \gamma_i = \arctan\left(\frac{y_i}{x_i}\right),$$
$$a_i(\theta) = \sqrt{A_i^2 \cos^2(\theta - \alpha_i) + B_i^2 \sin^2(\theta - \alpha_i)}, \tag{22}$$

where ρ_i is the intensity and A_i, B_i are the axes of the i^{th} ellipse, (x_i, y_i) is its center point, and α_i is its rotation angle relative to the x axis. The function J_1 stands for Bessel function of the first kind and the first order.

The k-space acquisition scheme is shown in Fig. 1. It includes 12 blades with 32 lines in the phase-encoding direction and 256 frequency samples in the readout direction for each blade, respectively. Two reconstructed 256 × 256 images are demonstrated in Fig. 3. The one shown in Fig. 3a is obtained by the regridding + FFT algorithm, and another, Fig. 3b, is reconstructed using the iterative optimization method. The images reconstructed from PROPELLER data by both techniques are almost equal to the image that would be obtained with a spin echo sequence (conventional k-space imaging) and approaches the quality of the original. However, due to the lack of data at the corners of k-space, the reconstructed images have some insignificant artifacts in the corners of the rectangular FOV (Fig. 3a). One may consider a circular FOV (or circular mask) for PROPELLER similar to radial or spiral acquisitions. The image in Fig. 3b has been reconstructed defining voxel unknown intensity inside the circular area of the square region.

We also used realistic phantoms and volunteers. Data were acquired on General Electric and Philips scanners. The agar phantom shown in Fig. 4 was reconstructed from data acquired on a GE 1.5 T scanner. The acquisition parameters are: 22 × 22 cm FOV, 4 mm slice thickness, TE/TR = 200/3000 ms, $b = 0$ attenuation constant, 24 blades with 16 phase lines and 256 readout samples. PROPELLER MRI is expected to work well for noisy or motion-affected realistic data (scanner vibrating during data acquisition). The next example in Fig. 5 was acquired on a Philips (Picker) 1.5 T scanner. The acquisition parameters are: 30 × 30 cm FOV, 5 mm slice thickness, TE/TR = 135/800 ms, $b = 0$ attenuation constant, 16 blades with 32 phase lines and 256 readout samples.

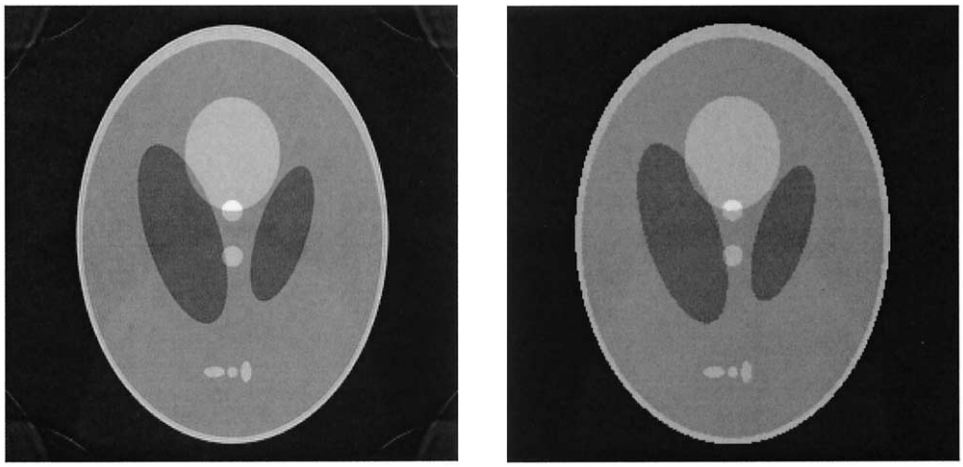

Fig. 3. The predicted image from computer-generated data obtained for Shepp-Logan phantom. The 256 × 256 image reconstructed (a) by regridding + FFT procedure; and (b) by iterative optimization algorithm.

4.2. Diffusion tensor imaging

Here, we show examples of two-dimensional image reconstructions using the above described algorithms.

The computer-generated phantom imitates two cylindrical elements of an anisotropic cardiac wall with an isotropic blood region inside each wall. The spin density of heart tissue and blood has values [0.8,1.0] and [0.6,1.0] for the upper and lower cylindrical elements, respectively (Fig. 6a). The structure of the diffusion tensor components D_{xx},D_{yy}, D_{xy} is shown in Fig. 6, b–d. The diffusion tensor eigenvalues of anisotropic myocardium [1.6,1.2] and isotropic blood [2.4] are for the upper element and [1.2,1.0] and [2.0] for the lower element, respectively (Fig. 6, e, 1st eigenvalue; f, 2nd eigenvalue). The eigenvector maps are represented in Fig. 6, g and i, 1st eigenvector, h and j, 2nd eigenvector. The attenuation constant, *b* value, is 1. Phantom resolution is 64 × 64 and the vector fields in Fig. 6, g and h have resolution 32 × 32 for convenient visualization. Three percent random noise was added to real and imaginary parts of the MR signal.

Fig. 7 demonstrates the results obtained by a conventional "regridding + FFT" technique. It is known that this method requires at least three diffusion-weighted datasets acquired with noncollinear diffusion gradient directions. Our reconstruction results with three datasets are represented in the form of the distribution of 1st and 2nd eigen-

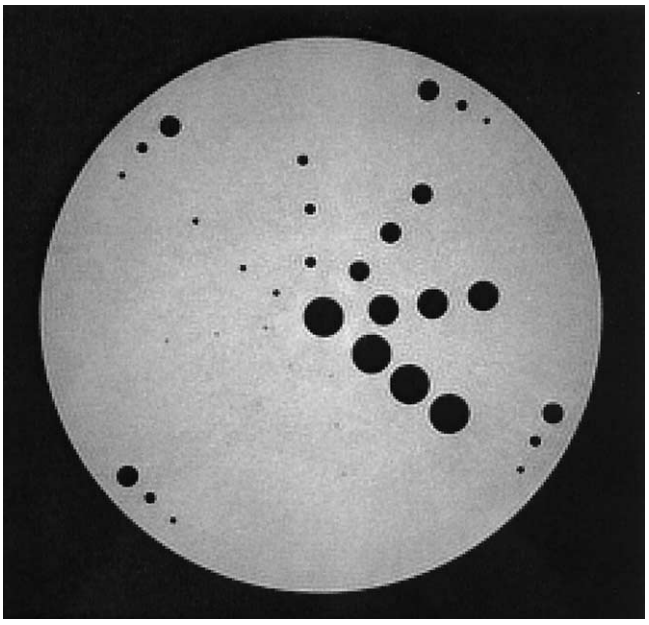

Fig. 4. The image of agar phantom from data acquired with GE scanner.

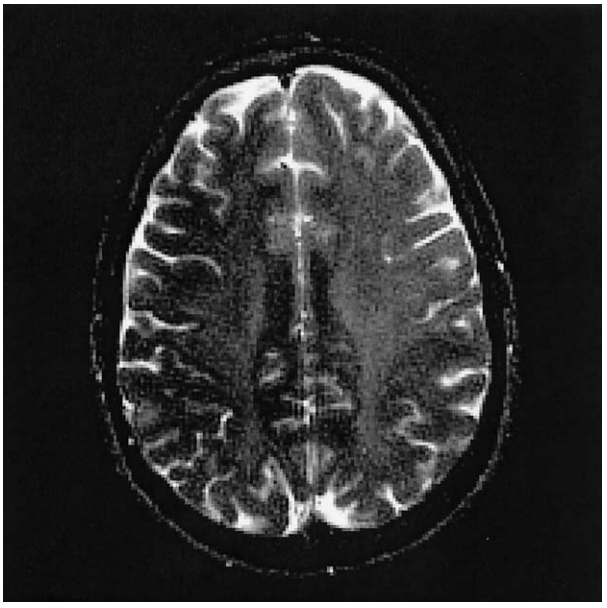

Fig. 5. Patient image reconstructed from data acquired with Picker (Philips) scanner.

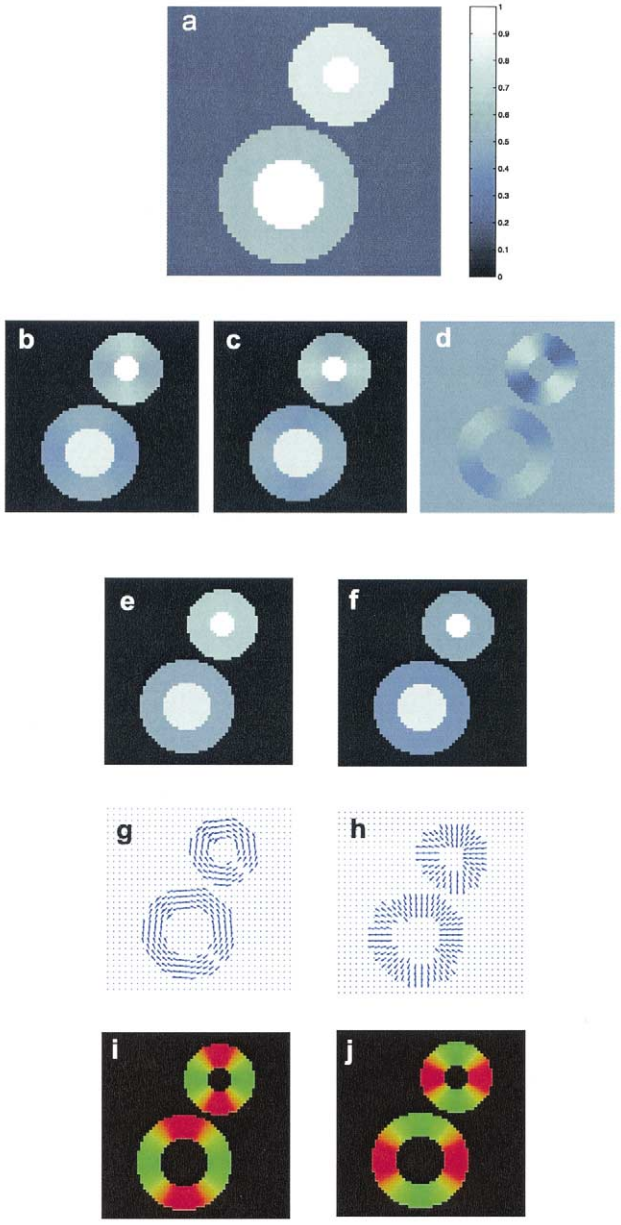

Fig. 6. The numerical phantom imitating two cylindrical cardiac walls with inner blood regions: (a) the proton density; DT components (b) D_{xx}, (c) D_{yy}, (d) D_{xy}; (e) 1st and (f) 2nd principal eigenvalues; (g and h) 1st and (h and j), 2nd principal vector maps, respectively. The colormaps in panels (i) and (j) describe horizontal vector component using red color and its vertical component using green color.

values and the maps of 1st and 2nd eigenvectors. The diffusion gradient directions, unit vectors ($\vec{\omega}_j$, j = 1,2,3), were chosen as [1,0], [1/$\sqrt{2}$, 1/$\sqrt{2}$], and [0,1].

The second example, Fig. 8, was obtained by the iterative extrapolation technique. One diffusion-weighted dataset is acquired. The PROPELLER *k*-space includes 12 blades, where [1,4,7,10] blades correspond to the first stationary gradient direction $\vec{\omega}_1$ = [1,0], [2,5,8,11] blades correspond to $\vec{\omega}_2$ = [1/$\sqrt{2}$, 1/$\sqrt{2}$], and [3,6,9,12] blades correspond to $\vec{\omega}_3$ = [0,1], respectively. For each set of blades we apply the

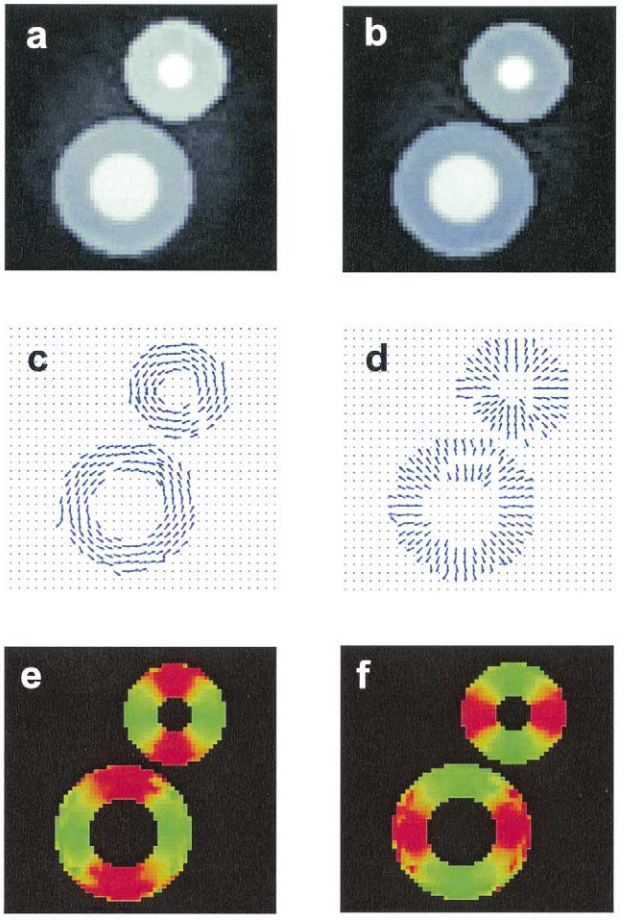

Fig. 7. The results of image reconstruction using regridding + FFT algorithm and three diffusion-weighted datasets: (a) 1st and (b) 2nd eigenvalues; (c and e) 1st and (d and f) 2nd eigenvectors, respectively.

Papoulis-Gerchberg iterative extrapolation algorithm. It requires 10 iterations to achieve a relative error of 0.05. The resultant DT parameters are obtained as described above for the regridding + FFT procedure.

The iterative optimization reconstruction was applied for measurements with a continuous rotating diffusion gradient. In our experiment we used only one dataset acquired with one diffusion gradient direction in each blade coordinate system. This direction was set up along blade readout. The iterative optimization took seven iterations to achieve a relative error of 0.05. The results are shown in Fig. 9.

The reconstructed DT parameters in Figs. 7–9 have the same level of accuracy. However, in the rotating gradient case (DTT MRI), one can significantly reduce the amount of data and the acquisition time which is three times less than conventional two-dimensional DTI. Also, it was shown earlier that DTT leads to a unique reconstruction of principal directions, whereas the conventional MRI technique (stationary diffusion gradients) leads to an ambiguous reconstruction of principal directions when the same number of measurements is used [7].

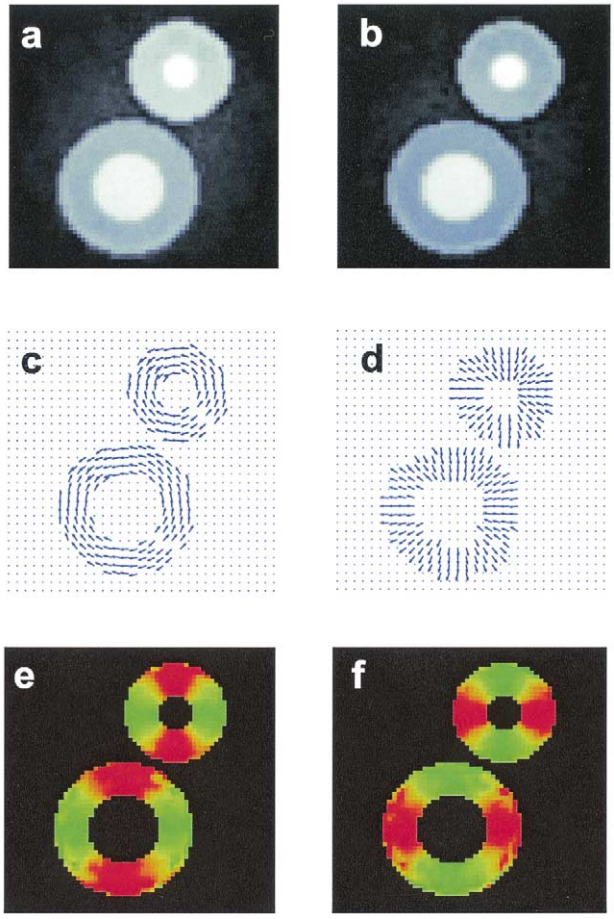

Fig. 8. The results of image reconstruction using iterative extrapolation algorithm and one diffusion-weighted dataset: (a) 1st and (b) 2nd eigenvalues; (c and e) 1st and (d and f) 2nd eigenvectors, respectively.

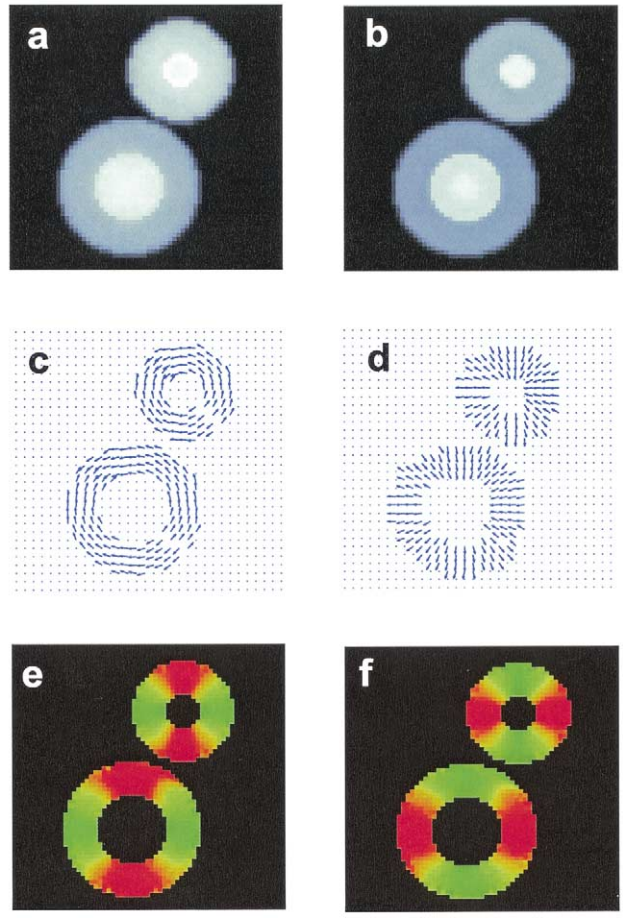

Fig. 9. The results of image reconstruction iterative optimization algorithm and one diffusion-weighted dataset: (a) 1st and (b) 2nd eigenvalues; (c and e) 1st and (d and f) 2nd eigenvectors, respectively.

5. Discussion

MR DT imaging covers two aspects of data acquisition: an acquisition strategy and the choice of a diffusion gradient encoding scheme. Existing DTI techniques often rely on uniform Cartesian *k*-space sampling using EPI sequences and apply diffusion gradients in fixed directions while an entire dataset is acquired. The number and the choice of noncollinear directions define a particular encoding scheme [1]. Any of these schemes requires the acquisition of at least three DW datasets in the two-dimensional case and six DW datasets in the three-dimensional case. DT images are calculated voxel-by-voxel and employ logarithms of DW and non-DW. In low spin density regions of the image, such techniques can lead to very noisy reconstructions. EPI-based imaging has low resolution and its image quality is seriously affected by the influence of magnetic susceptibility and eddy currents. Hence, new high-resolution and distortion-free diffusion imaging techniques are required for detailed clinical diagnostics. PROPELLER was proposed [11] as a two-dimensional acquisition scheme designed specifically to decrease the susceptibility and eddy current artifacts that occur in EPI.

Because PROPELLER DTI data acquisition can take 0.5-1 min per slice, it is worth considering methods that decrease acquisition time. The proposed method utilizing the Papoulis-Gerchberg extrapolation algorithm explores the idea of reducing the number of blades in the PROPELLER dataset and estimating the signal in the gaps between blades. Too little data leads to ambiguity and the loss of resolution. On the other hand, the overlap of PROPELLER blades at the *k*-space origin improves image SNR. This tradeoff makes it possible to maintain the quality of the resultant image. The extrapolation approach can be optimized with efficient *k*-space sampling, implementing accurate nonuniform fast Fourier analysis (NUFFT [28]), and improving the convergence of the reconstruction algorithm.

DTT MRI reconstructs tensor fields from scalar projections of the diffusion field. Acquiring field projections from multiple angles of view allows one to improve SNR and reduce bulk motion. Generally speaking, a tensor field can obviously have a very complicated structure, much more so than a scalar field. For instance, an arbitrary tensor field can be decomposed into rotational and irrotational tensor field

components [4]. The DTT approach exhibits an intrinsic flexibility in evaluating tensor fields with dominant contributions from the rotational component, which, for example, describes appropriately major properties of the human spine [18]. It was also shown that DTT can be an efficient tool for mapping the principal directions of fiber structures in muscle tissue and myocardium, if the principal values of those objects are known from side measurements [7]. Moreover, DTT MRI with rotating gradients provides a unique reconstruction of the principal diffusion directions, whereas conventional MRI acquisition with stationary gradients leads to ambiguous results in some situations. DTT uses a large number of angular projections to achieve needed image resolution and satisfy Nyquist criterion. Unfortunately, this feature is not easily implemented on existing MR hardware, which was designed primarily for nonrotating image acquisition.

The rotating blade acquisition of PROPELLER is not a true tomographic measurement. Although it acquires multiple blades, the PROPELLER scheme has a small number of strip segments, typically from 6 to 24. This makes the realization more practical. Each DW blade is produced by a fast spin-echo sequence, and the entire blade is rotated, rather than trying to rotate each line of *k*-space. PROPELLER DTT with rotating diffusion gradients is able to provide complete directional information for diffusion tensor reconstruction. This feature allows a dramatic reduction of the amount of DW data. In this approach, the reconstruction of the tensor field appears as a nonlinear inverse problem that can be solved by any iterative optimization method. Because the problem exhibits intrinsic ill-posedness, regularization should be applied to keep the solution in the vicinity of an a priori model estimate and to control its smoothness. The most challenging optimization problem within the optimization framework is storing the information in onboard memory. To reduce memory requirements, precomputing, on-fly calculations, and parallelization should be applied where possible.

In summary, the proposed method, DTT MRI with PROPELLER acquisition, promises to improve image quality when evaluating anisotropic tissues. The PROPELLER sequence has a natural immunity to artifacts caused by motion, eddy currents, and magnetic susceptibility effects. Rotating the diffusion gradient with the PROPELLER acquisition makes it possible to reduce the amount of data that must be acquired, thereby improving efficiency. In this work, we have tested several approaches to PROPELLER MRI with numerical simulations and phantom image acquisitions.

Acknowledgments

The authors thank Vladimir Panin (CPS Innovations, Inc.) for helpful discussions. This work was supported in part by the Director, Office of Science, Office of Biological and Environmental Research, Medical Sciences Division of the U.S. Department of Energy under contract DE-AC03-76SF00098 and by the US Department of Health and Human Services under The Biomedical Information Science and Technology Initiative, P20 HL68566-01.

References

[1] Shimony JS, McKinstry RC, Akbudak E, et al. Quantitative diffusion-weighted anisotropy brain MR imaging: normative human data and anatomic analysis. Radiology 1999;22:770–84.
[2] Tseng WY, Reese TG, Weisskoff RM, Brady TJ, Wedeen VJ. Myocardial fiber shortening in humans: Initial results of MR imaging. Radiology 2000;216:128–39.
[3] Ries M, Jones RA, Dousset V, Moonen CTW. Diffusion tensor MRI of the spinal cord. Magn Reson Med 2000;44:884–92.
[4] Gullberg GT, Gosh Roy D, Zeng GL, Alexander AL, Parker DL. Tensor tomography. IEEE Trans Nucl Sci 1999;46:991–1000.
[5] Gullberg GT, Defrise M, Panin VY, Zeng GL. Efficient cardiac diffusion tensor MRI by three-dimensional reconstruction of solenoidal tensor fields. Magn Reson Imag 2001;19:230–56.
[6] Panin VY, Zeng GL, Gullberg GT. An iterative approach to tensor tomography. Proc IEEE Nucl Sci Symp Med Imag Conf, Lyon, France, October 15–20, 2000, 15-272–76.
[7] Panin VY, Zeng GL, Defrise M, Gullberg GT. Diffusion tensor MR imaging of principal directions: A tensor tomography approach. Phys Med Biol 2002;47:2737–57.
[8] Glover GH, Pauly JM. Projection reconstruction technique for reduction of motion effects in MRI. Magn Reson Med 1992;28:275–89.
[9] Ahn CB, Kim HH, Cho ZH. High-speed spiral-scan echo planar NMR imaging. IEEE Trans Med Imag 1986;MI-5:2.
[10] Noel DC. Multi-shot rosette trajectories for spectrally selective MR imaging. IEEE Trans Med Imag 1997;16:372–7.
[11] Pipe JG. Motion correction with PROPELLER MRI: application to head motion and free-breathing cardiac imaging. Magn Reson Med 1999;42:963–9.
[12] Wajer FTAW, Coron A, Lethmate R, van Osch JAC, Martinez LT, Graveron-Demilly D, van Ormondt D. Accelerated Bayesian MR image reconstruction. In: Proceedings ProRISC, Workshop on Circuits, Systems, and Signal Processing. STW Technology Foundation, 2001, p. 721–27.
[13] Acar R, Vogel CR. Analysis of bounded variation penalty methods for ill-posed problems. Inverse Problems 1994;10:1217–29.
[14] Walle RV, Barett HH, Myers KJ, et al. Reconstruction of MR images from data acquired on a general nonregular grid by pseudoinverse calculation. IEEE Trans Med Imag 2000;19:1160–7.
[15] Dibos F, Koepfler G. Global total variation minimization. SIAM J Numer Anal 2000;37:646–64.
[16] Lee AT, Glover GH. Motion artifacts in fMRI: comparison of 2DFT with PR and spiral scan methods. Magn Reson Med 1995;33:624–35.
[17] Meyer CH, Hu BS, Nishimura DG, Macovski A. Fast spiral coronary artery imaging. Magn Reson Med 1992;28:202–13.
[18] Zhou XJ, Leeds NE, Pipe JG, Ma X. Diffusion-weighted imaging of the human spine using PROPELLER. In: Proc. 10th Meeting of International Society for Magnetic Resonance in Medicine, 2002, p. 1117.
[19] Mattiello J, Basser PJ, Le Bihan D. Analytical expresion for the b matrix in NMR diffusion imaging and spectroscopy. Magn Reson Imag 1994;37:292–300.
[20] Alexander AL, Hasan KM, Lasar M, Tsuruda JS, Parker DL. Analysis of partial volume effects in diffusion-tensor MRI. Magn Reson Med 2001;45:770–80.
[21] Jackson JI, Meyer CH, Nishimura DG, Macovski A. Selection of a convolution function for Fourier inversion using gridding. IEEE Trans Med Imag 1991;10:473–8.

[22] Zwaga JH, Wajer FT, de Beer R, Fuderer M, Mehlkopf AF, van Ormondt D. Improved Kaiser-Bessel window parameter selection for gridding. In: Proc. 6th Meeting of International Society for Magnetic Resonance in Medicine, 1998, p. 669.
[23] Chu YC, Rokhlin SI. Comparative analysis of through-transmission ultrasonic bulk wave methods for phase velocity measurements in anisotropic materials. J Acoust Soc Am 1994;95:3204–12.
[24] Ferreira PJ. Interpolation and the discrete Papoulis-Gerchberg algorithm. IEEE Trans Sign Proc 1994;42:2596–606.
[25] Portniaguine O, Zhdanov M. Focusing geophysical inversion images. Geophysics 1999;64:874–87.
[26] Rudin L, Osher S, Fatemi E. Nonlinear total variation based noise removal algorithms. Physica D 1992;60:259–68.
[27] Alexander AL, Ma X, Zong X, Pipe J. Diffusion-weighted PROPELLER imaging of the human brain at 3 Tesla. In: Proc. 10th Meeting of International Society for Magnetic Resonance in Medicine, 2002, p. 436.
[28] Fessler JA, Sutton BP. Nonuniform fast Fourier transforms using min-max interpolation. IEEE Trans Signal Proc 2002;51:560–74.